

■ Scientific Justification

1 Outflows and their Critical Role in Star Formation Feedback

Galaxies form from cooling gas that sinks to the centers of dark matter halos and self-gravitates to form stars (White & Rees, 1978). However, early models ran into the long-standing problem of “overcooling”, where the efficient accretion of gas into halos forms galaxies that are too massive and gas-rich (Dekel & Silk, 1986; White & Frenk, 1991).

Current galaxy formation models (e.g., Somerville & Davé, 2015) have addressed this problem by introducing feedback from supernova (SNe) explosions, which deposit enormous quantities of energy, enriched gas, and momentum into the surrounding interstellar medium (ISM; e.g. Thompson et al., 2005; Ostriker & Kim, 2022). This feedback is predicted to drive large-scale multi-phase galactic winds with mass loss rates comparable to the galaxy’s star formation rate (SFR), often quantified by the mass-loading factor $\eta_M \equiv \dot{M}_{\text{wind}}/\text{SFR}$ (Heckman et al., 1990; Strickland & Stevens, 2000; Strickland & Heckman, 2009). The presence of these galactic winds has been confirmed by observations of outflows in star-forming galaxies at high and low redshift (for reviews see Veilleux et al., 2005; Rupke, 2018).

Until recently, feedback models have generally adopted winds with large mass-loading (“ejective feedback”; Pillepich et al. 2018; Davé et al. 2019; Muratov et al. 2015; Pandya et al. 2021, 2020). However, this approach is now called into question. Observational measures of η_M are often orders-of-magnitude lower (Chisholm et al., 2017; McQuinn et al., 2019; Marasco et al., 2023) when compared to standard theoretical models. A potential resolution to this discrepancy is emerging from high resolution ISM patch simulations, which find a relatively low η_M , carried primarily by the cool phase ($T \sim 10^4$ K), and a very high *energy* loading ($\eta_E \equiv \dot{E}_{\text{wind}}/\dot{E}_{\text{SNe}}$) carried by the hot phase ($T \gtrsim 10^6$ K) (Fielding et al., 2018; Kim et al., 2020a; Li & Bryan, 2020). Hence, “preventive feedback” from heating (via thermalization of kinetic energy from SNe) may be more important than previously thought.

While observations aim to resolve this theoretical controversy, they still fall short. Some of the best measurements come from blueshifted ISM absorption lines observed with COS on HST (Heckman et al., 2015), but even these investigations must interpret observations using highly simplified analyses and many assumptions. The data alone provide little to no information about the density and velocity gradients in the outflows, the line-of-sight location of the gas, or the large scale geometry of outflows. And, critically, these measurements are only sensitive to the cool phase of the outflow. In turn, observations suffer from large systematic uncertainties on inferences of \dot{M}_{wind} , \dot{E}_{wind} , and the momentum flow rate, \dot{p}_{wind} .

We propose a new approach for leveraging observations and interfacing with theoretical models: we will generate mock observations directly from state-of-the-art outflow simulations (e.g., Abruzzo et al., 2022b). By simulating individual clouds entrained in a hot galactic wind, and combining them to make full-scale galactic outflows, we will maximize efficiency and flexibility, while retaining the sub-pc scale resolution required to capture the structure of gas in the cool phase. In this Legacy Theory proposal, we will compare mock observations to COS observations of star-forming galaxies in the low-redshift universe, deriving the most robust constraints to date on clumpy, multi-phase outflows and their role in feedback.

2 Multiphase Winds: Implications for Galaxy formation

To understand the properties of galactic winds and their role in galaxy formation we need accurate methods for modeling their launching mechanisms. The most robust approach to this galactic wind modeling challenge is via “small-scale” simulations that resolve patches of the ISM down to the \sim pc scales. These high resolutions are necessary to resolve the expanding SNe remnants and their interaction with the ISM, which is crucial to resolving the multiphase nature of galactic winds (e.g., Girichidis et al., 2016; Li et al., 2017; Kim et al., 2020a). The consensus picture emerging from these ISM patch simulations is that galactic winds likely have relatively low mass loading factors ($\eta_M \lesssim 1$), and that the hot phase ($T \sim 10^6$ K) carries most of the energy, while the cool phase ($T \sim 10^4$ K) carries most of the mass (Fielding et al., 2018; Kim et al., 2020b; Li & Bryan, 2020).

These multiphase winds may not eject much mass out of the galaxy, but the energy they contain can contribute to a *preventive* aspect of SNe feedback. Instead of only an ejective mode, energy flux from galactic winds can heat up and stir circumgalactic material, preventing further radiative cooling in the gas and limiting galactic accretion (Fielding et al., 2017; Voit et al., 2017). These SN-driven winds that escape from halos may also shock-heat gas beyond the CGM and thereby prevent cosmic accretion (Pandya et al., 2020). This new multiphase preventive wind paradigm is in direct conflict with standard single phase ejective models, but has recently been shown to be highly effective in regulating galaxy growth (Carr et al., 2022; Pandya et al., 2022; Smith et al., 2023)

How the cool and hot phases interact in a galactic wind was, until very recently, a major concern for multiphase wind models. The basis of this concern stemmed from the fact that observations showed the cool outflows leaving their host galaxies at hundreds of km s^{-1} , but all previous standard models predicted that the cool gas clumps should be mixed into the background hot medium and destroyed on a timescale much shorter than the ram pressure of the hot phase could accelerate it (e.g., Klein et al., 1994; Scannapieco & Brüggen, 2015; Schneider & Robertson, 2017). The resolution to this so called “entrainment in trouble” problem (Zhang et al., 2017), came from the realization that radiative cooling of the mixed gas in the wakes of large cool clouds can grow the clouds before they are mixed away (Gronke & Oh, 2018). State-of-the-art, extremely high resolution simulations of the cloud-wind interaction for individual clouds (see Figure 1, center) have further refined this simple picture into a detailed predictive model for the exchange of mass, momentum, and energy between the phases (e.g., Gronke & Oh, 2020; Fielding et al., 2020; Tan et al., 2021; Abruzzo et al., 2022a,b; Kanjilal et al., 2021). **Furthermore, these simulations make concrete predictions with critical implications for observations: many of the ions that are most readily-observable are found in the turbulent radiative mixing layers (TRMLs) that separate the cool and hot phases (Chen et al., 2022).**

These new insights have enabled, for the first time, the development of robust, self-consistent, multiphase galactic wind models. For example, Fielding & Bryan (2022) presented a semi-analytic model that encapsulates the launching mechanisms from the ISM patch simulations and the TRML-mediated cool cloud-hot wind interactions. This model is now able to predict for a galaxy of a given size and SFR the density, velocity, and temper-

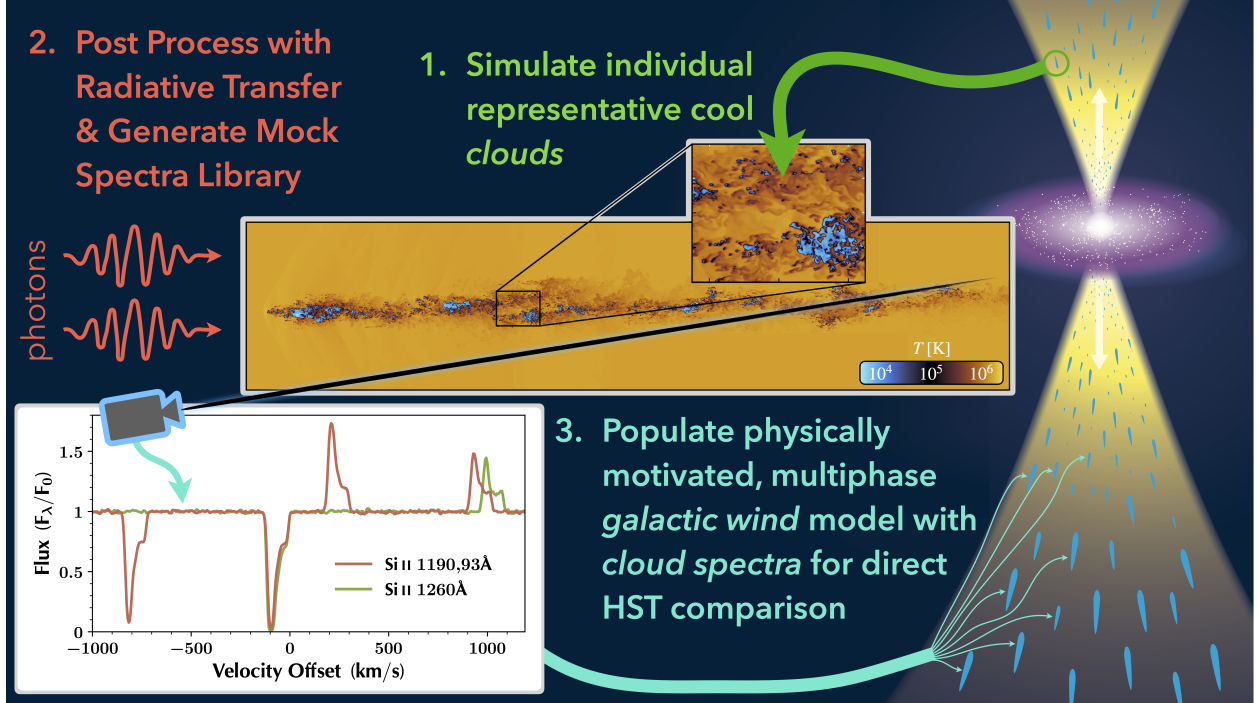


Figure 1: Schematic of our three-part method. The first part involves using a suite of extremely high resolution simulation of an individual cool cloud interacting with a supersonic hot wind. These simulations span the full range of cloud and wind properties that are expected for most galactic winds. The second part involves post-processing these simulations with full line radiative transfer to make mock line profiles for all simulated clouds. The final part involves combining cloud spectra according to predictions from a flexible physically motivated multiphase wind model to build a complete mock galactic wind spectrum for comparison to HST observations.

ature of the hot phase as a function of distance from the galaxy, as well as the properties of the cool clouds embedded within. These cool-cloud predictions depend primarily on four physically motivated parameters: the hot phase energy loading (η_E^{hot}), the cool phase mass loading (η_M^{cool}), the size distribution of the cool clouds (R_{cl}), and the wind opening angle (α). This proposal will demonstrate how changes to these physical parameters manifest observationally via spectral line profiles.

3 Challenges with the interpretation of observations

For decades, observational studies have attempted to constrain outflow models. Much of our knowledge comes from observations that use COS to measure blueshifted UV absorption lines in the spectra of star-forming galaxies (Heckman et al., 2015; Heckman & Borthakur, 2016; Chisholm et al., 2017; Xu et al., 2022, 2023). An example in Figure 2 (left) shows strong absorption in Si II, typical of low- z star-forming galaxies. These spectral features can be used to derive ionic column densities (typically Si, C, and O), characteristic outflow velocities v_{out} , and the maximum blueshifted velocity where the absorption meets the continuum (v_{max}). The mass loss rate is estimated as $\dot{M}_{\text{wind}} \approx \Omega \mu m_p N v_{\text{out}} R_{\text{wind}}$, where Ω is the solid angle subtended by the wind, μm_p is the mean mass per particle, N is the total column density of *all* outflowing gas, and R_{wind} is a characteristic radius of the outflow. Figure 2 (right) shows how the mass loading of the wind ($\eta_M \equiv \dot{M}_{\text{wind}}/\text{SFR}$) scales with galaxy stellar mass.

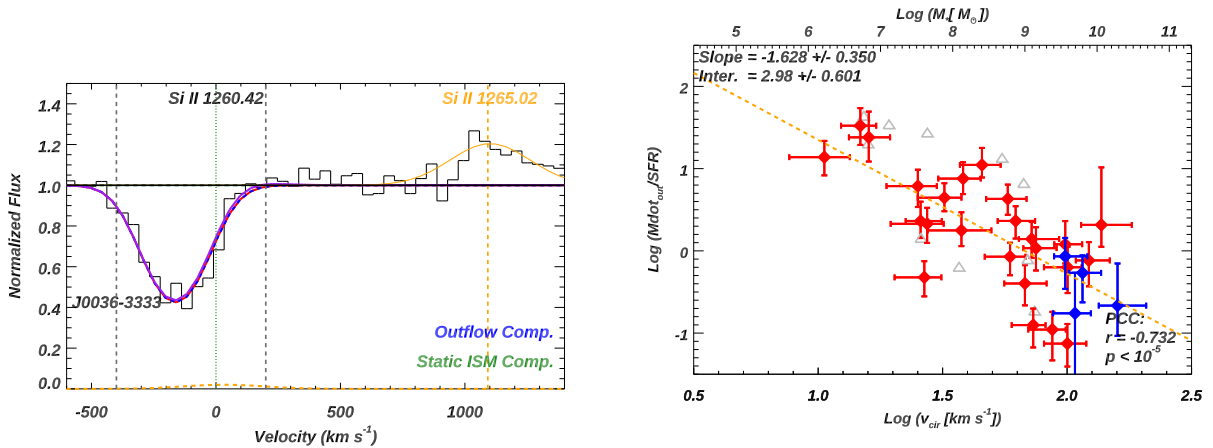


Figure 2: *Left*– A Si II line measured with COS shows strong blueshifted absorption, with a characteristic outflow velocity $v_{out} \sim 200 \text{ km s}^{-1}$ and a maximum outflow velocity, $v_{max} \sim 400 \text{ km s}^{-1}$. A fraction of photons absorbed in the Si II $\lambda 1260.4$ line are re-emitted through a fine structure level of the ground-state, resulting in Si II* $\lambda 1265.0$ emission. *Right*– The mass loading factor vs the circular velocity (bottom axis) and stellar mass (top axis). Red points are from the COS Legacy Archive Spectroscopic Survey (CLASSY; Berg et al., 2022; James et al., 2022), while blue points are another sample from Heckman et al. (2015). Open triangles represent galaxies that are large compared to the COS aperture. *Figures are taken from Xu et al. (2022).*

These measurements represent the standard method for comparing observational results with theoretical predictions. Yet efforts in this direction paint a somewhat muddled picture. For example, Xu et al. (2022) find agreement with recent semi-analytic or numerical simulations (Fielding et al., 2020; Gronke & Oh, 2020; Schneider et al., 2020; Kim et al., 2020b; Lochhaas et al., 2021), but only over limited parameter space. With models covering only a few sets of initial parameters (e.g., SFR, Ω , galaxy mass), it is difficult to find predictions that are appropriate for comparing to the range of galaxies that are observed with HST/COS.

Another reason that this comparison is so challenging is that the derivation of physical quantities from absorption spectra, as in Figure 2, requires many assumptions and approximations. For example, we generally do not know R_{wind} , or whether the outflow spans a large range of radii or a relatively thin shell. The data tell us little about the outflow solid angle, Ω , which may be biconical as in M82, or more spherical, as is implied by the high frequency of outflows detected in lower mass galaxies (e.g. Heckman et al., 2015). Additionally, column densities measured in individual metal ions that probe only the cool to intermediate temperatures must be scaled to infer the total gas column in all phases, N . Finally, for absorption line spectroscopy towards spatially extended galaxies, even column density and velocity are ill-defined. There can be many column densities along *one* line of sight, and regions with different radially-directed velocities can have the *same* projected, line-of-sight velocity. While spectral line profile fitting with sophisticated analytic models can account for some of these effects, these models are still highly idealized (e.g. Carr et al., 2018, 2021), and do not model the TRMLs where the UV spectral features are formed. **Ultimately, simulation-based techniques that are more rigorous, but also flexible, are needed to provide meaningful comparisons between theory and observation.**

Early efforts at mock spectroscopy of hydrodynamical simulations have attempted to

provide this more robust comparison. So far, *somewhat* realistic spectra have been produced, although they do not have the spatial resolution in the outflow to model the TRMLs (Mauerhofer et al., 2021; Katz et al., 2022). Nevertheless, these simulations have not been run past $z = 3$, making it difficult to compare them with high-quality UV spectra that are only available at low- z . Finally, as with most hydrodynamical simulations, there is only one instance of the astrophysics, and limited opportunity to tune the model.

4 A New Method for Modeling Outflow Spectra

Bearing in mind the limitations of the studies discussed above, we propose a novel method for constraining the physics of multiphase galactic winds. We will achieve this by combining mock spectra of individual state-of-the-art cloud-wind interaction simulations generated using full radiative transfer. These individual cloud spectra will be combined in a self-consistent manner following the predictions of a physically motivated multiphase galactic wind model. This process will enable us to directly explore how changes to the cloud properties and the global galactic wind parameters manifest in HST-like spectra. A schematic overview of our three-step method is shown in Figure 1.

4.1 Step 1: Simulations of Individual Clouds with a Variety of Properties

To make trustworthy predictions of galactic wind observations we need accurate simulations that reliably capture the detailed phase structure and morphology of individual cool clouds as they interact with the hot phase wind. We propose to use of a suite of 70 extremely high resolution `Enzo-E` (Bordner & Norman, 2018, enzo-e.readthedocs.io) simulations of *individual cool clouds* entrained in a hot wind (Abruzzo et al., 2022a,b). These simulations, each with ~ 20 snapshots in time, have been made available to us for this project (M. Abruzzo private comm.). The middle of Figure 1 shows one of these simulations and highlights the complex phase and clump structure of these systems. Overall, the simulation suite spans a broad range of physical parameters, varying the hot phase's velocity ($\sim 10\text{--}1000 \text{ km s}^{-1}$) and temperature ($\sim 10^5\text{--}10^7 \text{ K}$), and the size of the initial cool clouds ($\sim \text{pc--kpc}$). Over the duration of the simulations the relative velocity of the phases approaches zero as the cloud becomes entrained, which means this suite of simulations covers the full expected range of cloud properties at every point in a galactic wind. Furthermore, it has been shown that these simulations have fully converged temperature-density phase structures, which makes them ideal for making robust predictions. Lastly, these simulations were run in a unit system that allows them to be scaled to other pressures and metallicities for no additional cost.

4.2 Step 2: Cloud Spectral Library from Post-Processing Line Radiative Transfer

For each cloud snapshot, we will reprocess the data with Monte Carlo radiative transfer employing the publicly available code COLT (Smith et al., 2015, 2022, colt.readthedocs.io). We will obtain accurate ionization states with the iterative photoionization equilibrium modeling included in COLT. For this calculation, we will adopt the most up-to-date stellar population synthesis models (e.g. BPASS; Eldridge et al., 2017), externally illuminating the cloud with a range of surface intensities to determine the relative abundances of metal ions under consideration. We will then perform spatially- and spectrally-resolved radiative transfer to model the strong metal-line resonance transitions that are most commonly observed with

COS: Si II $\lambda\lambda$ 1190, 1193, λ 1260, λ 1302, λ 1526, Si III λ 1206, Si IV $\lambda\lambda$ 1393, 1403, C II λ 1334, C IV $\lambda\lambda$ 1548, 1550, and O I λ 1304. Each line is modeled by tracking incident non-ionizing UV photons, which are absorbed when they come into resonance with these transitions. Each photon scatters until it is absorbed by dust or escapes the cloud simulation domain, and doublet and fluorescent lines are modeled self-consistently together. The final post-processing output is a complete list of photons, including attributes such as their escaping frequencies and directions, which can then be used to build spectra for any configuration of viewing direction, spatial resolution, and aperture. We will perform this calculation for each cloud snapshot with conditions appropriate for a reasonable range of cloud locations and metallicities, thus enabling us to tractably combine and “observe” various wind models comprising potentially large numbers of clouds.

An example shown in Figure 1 demonstrates that a COLT model spectrum for a sight-line through one of our cloud simulations produces both absorption in resonant Si II $\lambda\lambda$ 1190, 1193 and λ 1260, as well as fluorescent emission that is coupled to these resonant lines (Si II* λ 1194, λ 1197, and λ 1265). As illustrated in Figure 3, the relative strengths between the absorption and emission are dependent on the spectroscopic apertures and the location of the outflow with respect to the background source (Prochaska et al., 2011; Scarlata & Panagia, 2015; Carr et al., 2018). Our modeling will be designed to account for these effects.

4.3 Step 3: Mock Spectra from our Flexible Multiphase Galactic Wind Model

Once we have generated the complete library of radiative transfer outputs for the full suite of simulated clouds we will then assemble them into complete mock galactic wind spectra. The cloud spectra will be combined according to the predictions from the open source semi-analytic multiphase galactic wind model presented by Fielding & Bryan (2022). As noted above, for a galaxy with a given size and SFR this model determines the physically consistent hot and cool phase properties as a function of galacto-centric distance once the 4 key model parameters have been set: (i) hot phase energy loading, η_E , (ii) cool phase mass loading, η_M , (iii) cool cloud size distribution, R_{cl} , and (iv) wind opening angle, α . For a given choice of parameters we can then populate the wind by assigning simulated clouds to the correct position and velocity in the wind. The spectrum of each cloud can then be coadded fully accounting for spatial overlap (e.g. shadowing) of the clouds and the viewing angle. (Further details are given in the Analysis Plan.) The power of this method comes from the underlying flexibility. Once the library of cloud spectra are generated from the pre-existing suite of simulations we will be able to rapidly explore how the spectra of galaxies launching winds with different physical properties differ. By leveraging the flexibility of this approach we will, for the first time, be able to concretely determine the observational signatures of physically consistent galactic wind models, and thereby dramatically increase the power of the vast suite of existing HST galactic wind observations for constraining the *physics* of galaxy formation.

5 Constraining Models with Mock Observations

In this section, we describe how we will compare our models to data. Above, we outlined a procedure for generating a library of synthetic galaxy spectra parameterized by a total

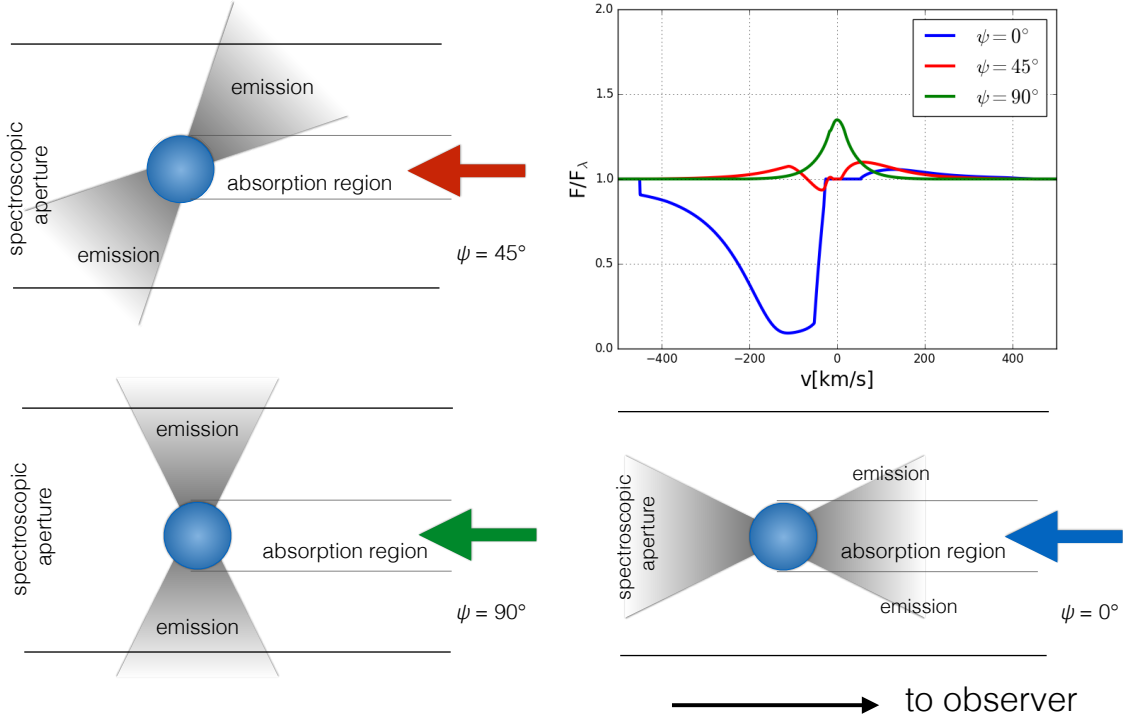


Figure 3: This cartoon sketch shows how orientation effects in a biconical outflow can impact the observed spectral lines. The red, blue, and green arrows indicate the line of sight to the star forming region, while the grey shaded regions show the biconical outflow that both absorbs and emits photons. An absorption line can only appear when the star-forming region is occulted by the outflow, yet emission can enter the spectroscopic aperture from regions not spatially coincident with the star-formation. The upper right panel shows how the spectra can change with viewing angle.

of 9 parameters: 4 physical parameters describing the wind (η_E^{hot} , η_M^{cold} , the cool cloud size distribution, R_{cl} , and the bicone opening angle, α), 4 parameters fixed by the galaxy being modeled (SFR, gas-phase metallicity, Z , the galaxy size R_* , and the physical size of the COS aperture R_{ap}), and lastly the orientation of the bicones relative to the line of sight, ψ . (A spherical, rather than biconical model will have $\alpha = 90^\circ$.) The data that we will fit with this model comprise the highest quality HST/COS spectra in the archive: approximately 50 galaxies, primarily from the COS Legacy Archive Spectroscopic Survey (Berg et al., 2022; James et al., 2022; Xu et al., 2022, 2023), with more being added every cycle. Critically, we will focus on directly observed metrics, such as equivalent width (EW) and v_{out} , rather than model-dependent, interpreted quantities like \dot{M}_{wind} . This process will unfold in two phases, which we describe in detail below.

5.1 Phase One: Data Exploration

The goal of this first phase is both to do an initial comparison of the predicted galaxy-scale model spectra with observations, as well as gain intuition into variations with viewing angle. Since COS observations semi-randomly sample sight lines (with a bias towards low-dust), this comparison will be statistical in nature. For a model, described by η_E^{hot} , η_M^{cold} , R_{cl} ,

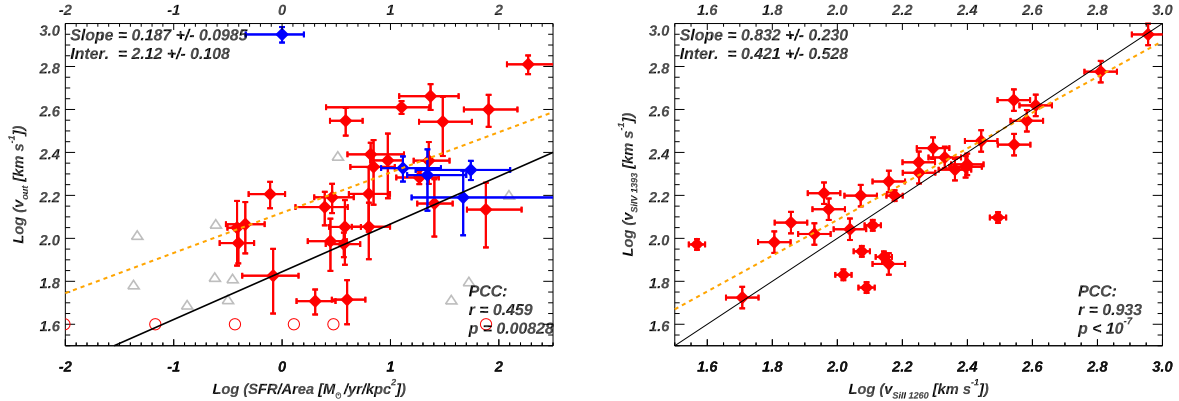


Figure 4: Characteristic outflow velocities (where optical depth in the outflow is the highest; v_{out}) are well-measured and not model-dependent. Red points represent the CLASSY sample, while blue points are from Heckman et al. (2015). In the left panel, open circles represent the galaxies that do not have outflows, while grey triangles show sources that are large relative to the COS aperture. The black solid line in the left panel is a model from Kim et al. (2020b), which matches the slope, but velocities are 3-5 times too low. In the right panel, the black line represents the 1:1 relation. In both panels, the orange dashed line is the best-fit. *Figure taken from Xu et al. (2022).*

α , SFR, Z , R_* , and R_{ap} to be a good description of the data, a random sampling of its low-dust sight lines (while varying the viewing angle, ψ) should yield equivalent widths and velocities that match the distribution means and dispersions seen in the observations. For this comparison, we will define a fiducial model with reasonable choices for the parameters listed above. Then, one-by-one we will perturb each above and below the fiducial value, arriving at a set of 17 outflow models. Each model will then be generated for 100 viewing angles, producing a library of 1,700 mock galaxy spectra covering the complete set of ions noted above. Finally, we will use automated routines to measure v_{out} , v_{max} , and residual flux in the absorption features, as well as FWHM and EW for both the emission and absorption lines. This library of measurements will be compared to data, using a wide variety of metrics such as those shown in Figure 4.

In addition to the comparison with observations, we can probe the data generation process more carefully by, for example, removing a subset of the clouds (e.g. those particularly close to, or far from the galaxy, or those with a certain range of bulk velocities) to see how their absence affects the resulting mock spectra. This data exploration will give us some sense of the robustness of the predictions as well as a better understanding of the physical cloud properties and the resulting observed absorption and emission features.

5.2 Phase two: Parameter Inference

The ultimate goals of this proposal are to (i) derive constraints on the underlying galactic wind model, and (ii) infer the wind parameters on a galaxy-by-galaxy basis. We will do this by using inference methods (e.g. an MCMC) to generate a posterior distribution of the wind parameters (η_E^{hot} , η_M^{cold} , R_{cl}), along with the opening angle α , and orientation ψ that are compatible with the spectrum for each galaxy. (The fixed parameters of our model,

SFR, Z , R_* , and R_{ap} are well constrained for the galaxies in our comparison sample.) We will use the pre-computed COLT spectra of individual clouds, and the same infrastructure that we developed and used for Phase 1. Additional model galaxy spectra will then be generated, expanding the spectral library and model parameter space covered in Phase 1. Then the simulated galaxy spectra will be compared directly to the COS spectra for all observed ions¹ to find the best fitting model. By design, this process will also allow us to explore degeneracies in the model, which will have critical implications for the way that data are interpreted in more traditional UV spectroscopic outflow observations.

We have outlined a method for generating high-fidelity mock observations of galactic winds through synthesis of theory and simulation. By modeling individual cool clouds with radiative transfer, then combining them into galactic-scale outflows based on a flexible wind model, we can explore how changes to physical parameters impact observable spectra. Our approach provides an end-to-end understanding of how starburst feedback shapes galaxies, from supernova explosions entraining cool clouds, to the radiation they emit and absorb, to the outflows that regulate star formation. Comparison with COS observations will enable the most robust constraints on whether winds are ejective or preventive. At the completion of this project, we will release our library of mock spectra to the public, enabling new and innovative science from the broader community.

■ Analysis Plan

A new method for creating high-fidelity mock spectra

As noted in the science justification, the simulations require sub-pc scale resolution, but we are aiming to produce spectra that can be compared to galaxy-wide observations. To make this problem computationally tractable, we have devised a new procedure to build a galaxy-wide model by adding spectra through individual clouds. In broad strokes, this is illustrated in Figure 1. In more detail, the coaddition of individual cloud spectra will require careful attention and organization as we build and test a rigorous infrastructure. The combination of spectra will account for the following features:

Cloud and Galaxy Orientation: When the cool clouds are assigned to a location in the hot wind, their velocity vectors and incident radiation field will be oriented radially. Yet this direction does not necessarily align with the line-of-sight. Therefore, each cloud will have its spectrum extracted from the COLT output for the line-of-sight towards the observer. Likewise, the clouds will be placed in a variety of large scale geometries, including spherically symmetric and bicones with a range of opening angles and orientations.

Scattered Emission: As illustrated in Figure 3, it is possible for an outflow to be oriented in the plane of the sky with little to no covering of the stellar spectrum. In this case, there is little to no absorption. Nonetheless, the photons absorbed by the outflow in both the

¹For this investigation, we will correct the observed spectra to remove the $v \sim 0$ ISM component that is not part of the outflow, as is done in Xu et al. (2022, 2023).

resonant and fluorescent transitions can be seen in *emission*. Therefore, for clouds that do not cover the source, but do fall in the spectroscopic aperture, we will include the emission component only.

Shadowing: When clouds overlap along the line of sight, we will fully account for the effect of shadowing. The absorption spectra will be added in optical depth space, tracking the covering fractions for each individual cloud and the regions where they overlap. For example, for two clouds, we have C_f^1 and C_f^2 as the fraction of the continuum covered by clouds 1 and 2 only, and C_f^{12} as the area covered by both clouds. The resulting spectrum would be represented by $I(v) = 1 - C_f^1(1 - e^{\tau^1(v)}) - C_f^2(1 - e^{\tau^2(v)}) - C_f^{12}(1 - e^{\tau^1(v)+\tau^2(v)})$, where v is the line-of-sight velocity and $\tau^1(v)$ and $\tau^2(v)$ are the optical depths through each cloud. We will generalize this arithmetic to an arbitrary number of clouds. Validation tests will verify this procedure by running COLT on a small set of clouds that overlap along the line of sight.

Spectroscopic Apertures: The comparison galaxies are observed by COS through a 2.5'' diameter aperture. To create models relevant to the observations, we will only combine cloud spectra that would fall within the aperture. At $z = 0.1$, typical of COS samples, this aperture subtends 4.7 kpc. We will also include the vignetting outside the central 1'' of the aperture, down-weighting cloud spectra that fall at larger radii.

Scattering Between Clouds: Because the turbulent velocities in the clouds are small relative to the velocity in the wind, scattering between the clouds can be ignored. This occurs because we expect the Sobolev approximation to be valid throughout our simulated galaxies (Sobolev, 1960). In other words, photons scattered in an individual cloud will be out of resonance with other clouds. We expect that the velocity gradient in the outflow is steep enough that this criterion will be met most of the time. We will track whether individual clouds meet the Sobolev criterion, and carry out validation tests for this assumption, thereby ensuring the fidelity of our spectral co-addition.

Relevant Data Sets

Since the installation of COS, HST has obtained high-resolution (the M-gratings), high signal-to-noise UV spectroscopy of star-forming galaxies in more than 20 programs. In Cycle 27, the COS Legacy Spectroscopic Survey (CLASSY) assembled a sample of the highest quality spectra in the archive, and supplemented these with new COS observations to complete the UV spectroscopic wavelength coverage. The resulting spectral atlas is presented in Berg et al. (2022), and comprises 45 galaxies.

In addition, we will supplement this sample with eight galaxies where the COS data are sufficient for outflow analyses. Of these, five are Lyman Break Analog galaxies from Heckman et al. (2015), and were included by Xu et al. (2022) in the first CLASSY paper presenting outflows. The remaining three are from HST GO 15881 (PI Stark; two metal poor galaxies), and GO 16071 (PI Kumari; one blue compact dwarf). In total, the comparison sample comprises 53 galaxies. Likewise, any additional high-resolution and high signal-to-noise spectroscopy in Cycle 31 (and perhaps Cycle 32) will be publicly available by Years 2 and 3 when we compare our models with observations.

Project Timeline

This proposal presents a PhD-thesis-scale project, so we outline a three year timeline for completing the work. Of note, the PhD student is already part of the project, and is a co-I on this proposal. They have just completed their second year, and will be ready to begin work on this program in the fall of 2023. The timeline is described below.

Year 1: The emphasis in the first year of the program will be on building and testing the tools that we will use to combine the individual cloud spectra. In detail, the PhD student will use the cloud simulations that have been made available to our team (Abruzzo et al., private comm.). They will learn how to use COLT to produce mock spectra from individual clouds (3 months), develop routines to assign the clouds to locations in the hot wind outflow (4.5 months), and work with the rest of the team to carry out quality assurance tests to verify that the technical details noted above have been correctly modeled (4.5 months). In parallel, a few members of our team will carry out a small number of additional cloud simulations to test the impact of varying cloud parameters beyond those already done.

Year 2: In the second year, the PhD student will prepare a manuscript to illustrate our spectral modeling method developed in Year 1. In this paper, they will present results from just one model, along with the validation tests (3 months). Then, they will move on to Phase 1 of the data comparison, where we will explore distributions of directly observed (model-independent) absorption and fluorescent emission features. They will first build a spectral library for the set of models discussed in §5.1 (2 months). Then, using automated tools, they will measure the equivalent widths, velocities, and FWHM for the resonant absorption lines and the fluorescent emission features (2 months), and finally they will compare with observational results, interpreting the agreements and discrepancies, while preparing a manuscript for publication (5 months). The measurements from COS spectra have been provided to our team (Xu, X., private comm.).

Year 3: The third year of the project, the PhD student will move on to Phase 2 of the data comparison, where we aim to infer the parameters describing the wind model. They will first build a pipeline (4 months) for model fitting that can automatically draw on the library of computed spectra (expanding as necessary), and for each galaxy with known properties (SFR, galaxy size, COS aperture size), draw a sample from the prior distribution of unknown wind parameters, and then determine a likelihood of the fit based on a comparison of the spectrum. This pipeline will then be used in a Bayesian sampling algorithm to constrain the wind parameters that are compatible with the observed galaxy (4 months). This will be repeated for each galaxy and paper will be written (4 months) describing the distribution of wind parameters inferred this way, exploring any correlations, and discussing the result in terms of the ejective and preventive pictures for galaxy formation.

References

Abruzzo, M. W., Bryan, G. L., & Fielding, D. B. 2022a, ApJ, 925, 199

Abruzzo, M. W., Fielding, D. B., & Bryan, G. L. 2022b, arXiv e-prints, arXiv:2210.15679

- Berg, D. A., James, B. L., King, T., et al. 2022, The Astrophysical Journal Supplement Series, 261, 31
- Bordner, J., & Norman, M. L. 2018, arXiv e-prints, arXiv:1810.01319
- Carr, C., Bryan, G. L., Fielding, D. B., Pandya, V., & Somerville, R. S. 2022, arXiv e-prints, arXiv:2211.05115
- Carr, C., Scarlata, C., Henry, A., & Panagia, N. 2021, The Astrophysical Journal, 906, 104
- Carr, C., Scarlata, C., Panagia, N., & Henry, A. 2018, The Astrophysical Journal, 860, 143
- Chen, Z., Fielding, D. B., & Bryan, G. L. 2022, arXiv e-prints, arXiv:2211.01395
- Chisholm, J., Tremonti, C. A., Leitherer, C., & Chen, Y. 2017, MNRAS, 469, 4831
- Chisholm, J., Tremonti, C. A., Leitherer, C., & Chen, Y. 2017, arXiv.org
- Davé, R., Anglés-Alcázar, D., Narayanan, D., et al. 2019, MNRAS, 486, 2827
- Dekel, A., & Silk, J. 1986, ApJ, 303, 39
- Eldridge, J. J., Stanway, E. R., Xiao, L., et al. 2017, Publications of the Astronomical Society of Australia, 34, e058
- Fielding, D., Quataert, E., & Martizzi, D. 2018, MNRAS, 481, 3325
- Fielding, D., Quataert, E., McCourt, M., & Thompson, T. A. 2017, MNRAS, 466, 3810
- Fielding, D. B., & Bryan, G. L. 2022, ApJ, 924, 82
- Fielding, D. B., Ostriker, E. C., Bryan, G. L., & Jermyn, A. S. 2020, ApJ, 894, L24
- Girichidis, P., Walch, S., Naab, T., et al. 2016, MNRAS, 456, 3432
- Gronke, M., & Oh, S. P. 2018, MNRAS, 480, L111
—. 2020, MNRAS, 492, 1970
- Heckman, T., Alexandroff, R., Borthakur, S., Overzier, R., & Leitherer, C. 2015, ApJ, 809, 147
- Heckman, T. M., Armus, L., & Miley, G. K. 1990, The Astrophysical Journal Supplement Series, 74, 833
- Heckman, T. M., & Borthakur, S. 2016, The Astrophysical Journal, 822, 9
- James, B. L., Berg, D. A., King, T., et al. 2022, The Astrophysical Journal Supplement Series, 262, 37

- Kanjilal, V., Dutta, A., & Sharma, P. 2021, MNRAS, 501, 1143
- Katz, H., Garel, T., Rosdahl, J., et al. 2022, Monthly Notices of the Royal Astronomical Society, 515, 4265
- Kim, C.-G., Ostriker, E. C., Somerville, R. S., et al. 2020a, ApJ, 900, 61
- Kim, C.-G., Ostriker, E. C., Fielding, D. B., et al. 2020b, ApJ, 903, L34
- Klein, R. I., McKee, C. F., & Colella, P. 1994, ApJ, 420, 213
- Li, M., & Bryan, G. L. 2020, The Astrophysical Journal, 890, L30
- Li, M., Bryan, G. L., & Ostriker, J. P. 2017, ApJ, 841, 101
- Lochhaas, C., Thompson, T. A., & Schneider, E. E. 2021, MNRAS, 504, 3412
- Marasco, A., Belfiore, F., Cresci, G., et al. 2023, A&A, 670, A92
- Mauerhofer, V., Verhamme, A., Blaizot, J., et al. 2021, A&A, 646, A80
- McQuinn, K. B. W., van Zee, L., & Skillman, E. D. 2019, ApJ, 886, 74
- Muratov, A. L., Kereš, D., Faucher-Giguère, C.-A., et al. 2015, MNRAS, 454, 2691
- Ostriker, E. C., & Kim, C.-G. 2022, ApJ, 936, 137
- Pandya, V., Somerville, R. S., Anglés-Alcázar, D., et al. 2020, ApJ, 905, 4
- Pandya, V., Fielding, D. B., Anglés-Alcázar, D., et al. 2021, MNRAS, 508, 2979
- Pandya, V., Fielding, D. B., Bryan, G. L., et al. 2022, arXiv e-prints, arXiv:2211.09755.
<https://arxiv.org/abs/2211.09755>
- Pillepich, A., Springel, V., Nelson, D., et al. 2018, MNRAS, 473, 4077
- Prochaska, J. X., Weiner, B., Chen, H.-W., Mulchaey, J., & Cooksey, K. 2011, ApJ, 740, 91
- Rupke, D. S. N. 2018, Galaxies, 6, 138
- Scannapieco, E., & Brüggen, M. 2015, ApJ, 805, 158
- Scarlata, C., & Panagia, N. 2015, Astrophysical Journal, 801, 43
- Schneider, E. E., Ostriker, E. C., Robertson, B. E., & Thompson, T. A. 2020, ApJ, 895, 43
- Schneider, E. E., & Robertson, B. E. 2017, ApJ, 834, 144
- Smith, A., Safranek-Shrader, C., Bromm, V., & Milosavljević, M. 2015, Monthly Notices of the Royal Astronomical Society, 449, 4336

- Smith, A., Kannan, R., Tacchella, S., et al. 2022, MNRAS, 517, 1
- Smith, M. C., Fielding, D. B., Bryan, G. L., et al. 2023, arXiv e-prints, arXiv:2301.07116
- Sobolev, V. V. 1960, Moving Envelopes of Stars
- Somerville, R. S., & Davé, R. 2015, Annual Review of Astronomy and Astrophysics, 53, 51
- Strickland, D. K., & Heckman, T. M. 2009, The Astrophysical Journal, 697, 2030
- Strickland, D. K., & Stevens, I. R. 2000, Monthly Notices of the Royal Astronomical Society, 314, 511
- Tan, B., Oh, S. P., & Gronke, M. 2021, MNRAS
- Thompson, T. A., Quataert, E., & Murray, N. 2005, ApJ, 630, 167
- Veilleux, S., Cecil, G., & Bland-Hawthorn, J. 2005, Annual Review of Astronomy and Astrophysics, 43, 769
- Voit, G. M., Meece, G., Li, Y., et al. 2017, ApJ, 845, 80
- White, S. D. M., & Frenk, C. S. 1991, ApJ, 379, 52
- White, S. D. M., & Rees, M. J. 1978, Monthly Notices of the Royal Astronomical Society, 183, 341
- Xu, X., Heckman, T., Henry, A., et al. 2022, The Astrophysical Journal, 933, 222
- . 2023, The Astrophysical Journal, 948, 28
- Zhang, D., Thompson, T. A., Quataert, E., & Murray, N. 2017, MNRAS, 468, 4801